

# The Control of Sensing Properties for Sm<sub>2</sub>O<sub>3</sub>-ZrO<sub>2</sub> Humidity Sensor

Chunjie Wang<sup>1, a</sup> and Yue Wang<sup>1, b \*</sup>

<sup>1</sup>College of Engineering, Bohai University, Jinzhou, 121013, China

<sup>a</sup> cjwang@foxmail.com, <sup>b</sup> wangsuiyue@foxmail.com

**Keywords:** Sensor; Humidity; Control; Doped

**Abstract.** The humidity sensitive characteristics of 10 mol% Sm<sub>2</sub>O<sub>3</sub> doped ZrO<sub>2</sub> sensors were investigated in the relative humidity range from 11% to 95% with various frequencies under 25 °C. Qualitative analyses indicate that the humidity sensing properties of Sm<sub>2</sub>O<sub>3</sub> - ZrO<sub>2</sub> can be controlled by doping Sm<sub>2</sub>O<sub>3</sub> with content is 10 mol%. The corresponding sensor shows excellent performance at 100 Hz, such as high humidity sensitivity and fast response-recovery time. Both properties are much better than those of pure ZrO<sub>2</sub> sensor. Furthermore, the resistance of sensor drops by about four orders of magnitude with relative humidity increasing.

## Introduction

Recent years, humidity sensors as an important sensor have attracted much attention due to their broad applications in various fields [1, 2]. Generally, the qualified humidity sensing materials should possess some characteristics, for example, high sensitivity, good chemical and physical stability, rapid response and recovery time, and low hysteresis [3, 4]. As an essential element of sensors, hence, sensing materials should be improved with high sensitivity and reliability in order to meet the increasing requirements. There are two types sensing material for humidity sensors: organic polymer films and porous ceramic films [5]. The main disadvantages for both materials are the low operation temperature, poor physical and chemical stability, and the dull response and recovery time.

Nano-sized thin films are optimal candidates for humidity sensor for their high surface area, and the large surface area facilitates the adsorption process of water molecules. ZrO<sub>2</sub> as humidity sensing material becomes heatedly discussed topics in recent years. The main disadvantage of ZrO<sub>2</sub> is the longer response and recovery time, which leads to the pure ZrO<sub>2</sub> sensor can not meet the human's requirements. Due to the remarkable physicochemical activity, rare earth materials are widely used to improve the performance of sensors. Cosentino et al devoted their works to the zirconia-titania porous ceramics for humidity sensors [6]. Su et al studied the Y<sup>3+</sup> and Mg<sup>2+</sup> doped zirconia thick film humidity sensors [7]. Wang et al reported the properties of nano-structured films humidity sensor with commercial ZrO<sub>2</sub> nanoparticles [8]. To the best of our knowledge, however, the performance of humidity sensors controlled by doping Sm<sup>3+</sup> for ZrO<sub>2</sub> sensor has not been reported.

Herein, nano-sensor material of 10 mol% Sm<sub>2</sub>O<sub>3</sub> doped ZrO<sub>2</sub> were synthesized via hydrothermal method. The physical and chemical properties of the as-synthesized powders, the sensing performance of corresponding sensor were investigated in the relative humidity range from 11% to 95% at room temperature. The main purpose of this study is tried to control the humidity sensing performance of the humidity sensor by doping rare earth materials.

## Experimental

Nanoparticles of 10 mol% Sm<sub>2</sub>O<sub>3</sub> doped ZrO<sub>2</sub> were synthesized via the conventional hydrothermal method. Detailed steps can be reference [8]. For comparison, the pure ZrO<sub>2</sub> nanopowders were synthesized by the same procedure. The crystalline phases of nanocrystalline powders were identified by powder X-ray diffraction (XRD, Bruker D8 Focus powder X-ray diffractometer) using Cu K $\alpha$

radiation ( $\lambda=1.5406 \text{ \AA}$ ) with a scanning rate of  $5^\circ\text{min}^{-1}$ . The operation voltage and current were maintained at 40 kV and 40 mA, respectively [8]. The mean particle size of powders ( $D$ ) was determined by Scherrer's equation.

## Results and Discussion

For both samples, the thermal behaviors were investigated by TG/DSC, as shown in Fig. 1. It can be noted from Fig. 1, the overall mass loss is about 1.52% for 10 mol%  $\text{Sm}_2\text{O}_3$  doped  $\text{ZrO}_2$ . While for pure  $\text{ZrO}_2$ , the whole mass loss is 1.43%. The mass losses for both samples mainly came from the decomposition of organic substances and the evaporation of physically absorbed water [8]. In the case of DSC curves, both samples have an exothermic peak at about  $90^\circ\text{C}$ , which can be due to the elimination of residual organic substances [9]. Moreover, another exothermic peak near  $1100^\circ\text{C}$  is resulted from the grain coarsening [10], and the temperature of this peak for 10 mol%  $\text{Sm}_2\text{O}_3$  doped  $\text{ZrO}_2$  is lower than that of pure  $\text{ZrO}_2$ .

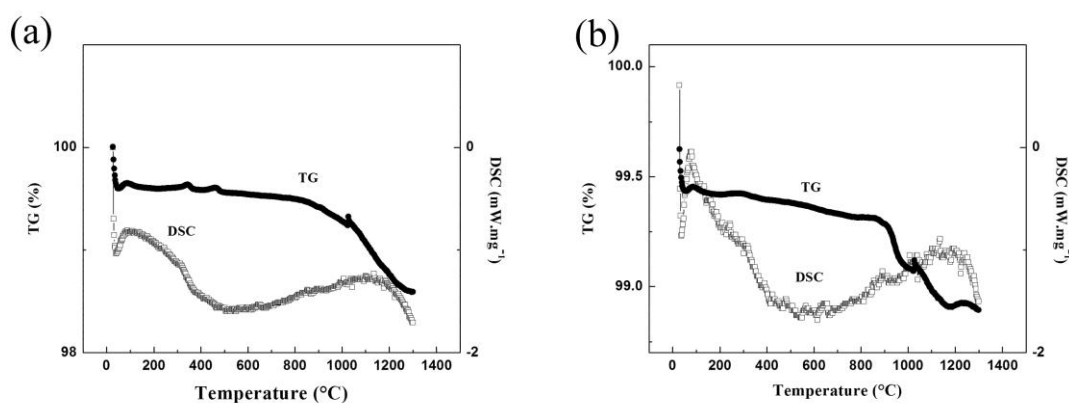


Figure 1. TG and DSC curves of as-synthesized 10 mol%  $\text{Sm}_2\text{O}_3$  doped  $\text{ZrO}_2$  (a) and  $\text{ZrO}_2$  (b) powders.

The phase structures of the as-prepared products for both samples were examined by XRD. From Fig. 2, both as-synthesized products show a typical cubic structure [JCPDS 78-1291]. The diffraction peaks locating at  $30.1^\circ$ ,  $34.9^\circ$ ,  $50.2^\circ$  and  $59.6^\circ$  can be well assigned to the (111), (200), (220) and (311) reflections, respectively. No other phase structure can be observed which implying the final products are pure and no other impure. For the peak position, compared to pure  $\text{ZrO}_2$ , 10 mol%  $\text{Sm}_2\text{O}_3$  doped  $\text{ZrO}_2$  is shift to low angle which indicating the variation of lattice parameters. This fact can be explained as following:  $\text{Sm}_2\text{O}_3$  has been dissolved in the  $\text{ZrO}_2$  crystal lattice through substitution solid solution [11]. The ionic radius of  $\text{Sm}^{3+}$  (0.106 nm) is much larger than that of  $\text{Zr}^{4+}$  (0.072 nm). The substitution of  $\text{Zr}^{4+}$  by  $\text{Sm}^{3+}$  will leads to the lattice distortion [12]. This is the reason for the peak position of 10 mol%  $\text{Sm}_2\text{O}_3$  doped  $\text{ZrO}_2$  lower than that of  $\text{ZrO}_2$ . In addition, the crystalline sizes and specific surface areas of both samples were also investigated. The calculated crystal sizes for both samples are 15.32 and 24.61 nm, respectively. Furthermore, in this study, the as-synthesized 10 mol%  $\text{Sm}_2\text{O}_3$  doped  $\text{ZrO}_2$  powders has a high specific surface area of  $106.53 \text{ m}^2 \text{ g}^{-1}$ , which is larger than that of pure  $\text{ZrO}_2$  ( $86.43 \text{ m}^2 \text{ g}^{-1}$ ). The high specific surface area is beneficial to the performance of humidity sensor.

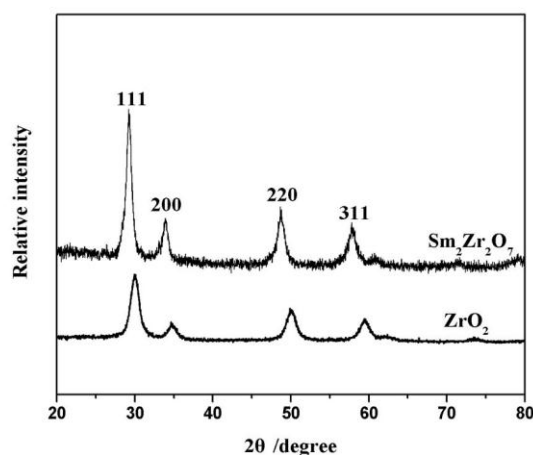


Figure 2. XRD patterns of as-prepared products of 10 mol%  $\text{Sm}_2\text{O}_3$  doped  $\text{ZrO}_2$  and pure  $\text{ZrO}_2$ .

In order to study the influence of humidity sensing properties for doping, the relationship between the resistance variation and relative humidity (RH) were measured under different frequencies at 25 °C. It can be observed in Fig. 3, for the doped sensor, the resistance of sensor at low frequency region (10 and 100 Hz) varied three orders of magnitude as the relative humidity changed from 11 to 95% RH, while the impedance only changed two orders of magnitude at 100 Hz at the same relative humidity range mentioned above. The higher the sensing properties are, the better the linear relation of resistance vs. RH will be. Furthermore, it can be obviously noted from Fig. 3, the humidity sensing property of doped sample is better than that of pure  $\text{ZrO}_2$  with the frequency is 100 Hz. The reason can be explained as the mechanism of depletion type adsorption of semiconductor materials: for the pure  $\text{ZrO}_2$  humidity sensor, electrons as the carrier have an important role on the conduction process. The addition of low valent cation dopants will lead to the concentration of elections decrease, indicating that conductivity declining and impedance becoming larger [13].

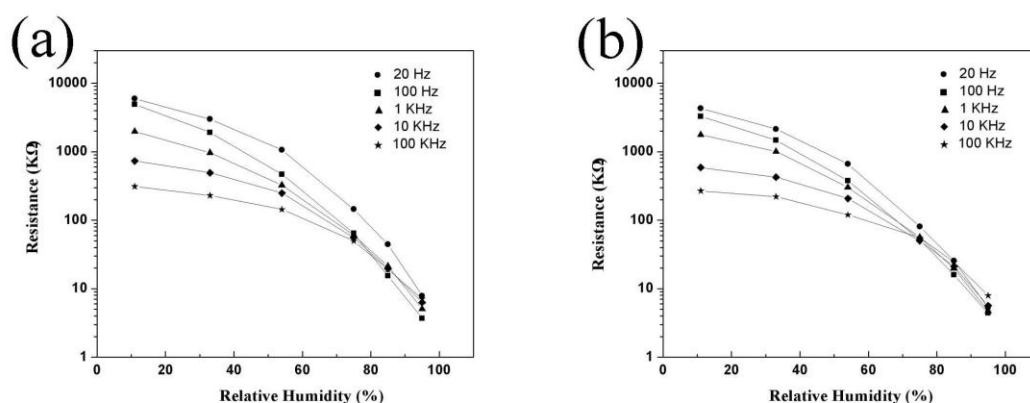


Figure 3. Resistance vs. RH plots of 10 mol%  $\text{Sm}_2\text{O}_3$  doped  $\text{ZrO}_2$  (a) and  $\text{ZrO}_2$  (b) nanopowders sensor at various frequencies.

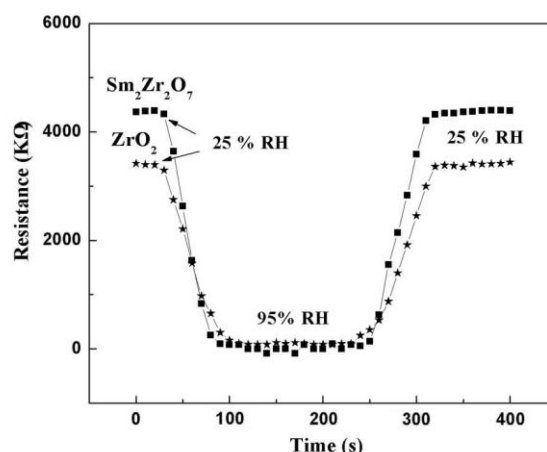


Figure 4. Response and recovery characteristics of 10 mol%  $\text{Sm}_2\text{O}_3$  doped  $\text{ZrO}_2$  and  $\text{ZrO}_2$  nanopowders sensor measured at 100Hz.

The response and recovery time of both samples were further investigated to evaluate the performance of sensor, as shown in Fig. 4. The sensor is putted from initial atmosphere (25% RH) to final atmosphere (95% RH) and transferred back to investigate the response and recovery time. From Fig. 4, the response time of doped sensor is about 50 s, and the recovery time is about 60 s. For the pure  $\text{ZrO}_2$ , however, the response and recovery time are 70 and 90 s, respectively. This fact indicating that the humidity sensing property of  $\text{ZrO}_2$  sensor can be effety improved by doping  $\text{Sm}_2\text{O}_3$ .

Rare earth materials have widely used to control the performance of functional materials. The addition of low valent cation dopants can result in the change of the elections concentration. In addition, the adsorption process of water molecules is more important for the properties of humidity sensor [14]. When the relative humidity is low, few molecules will be adsorbed on the sensor's surface. The electrolytic conduction will be influenced by the humid atmosphere on the surface. In this case, two cases will improve the electrolytic conduction: the high local charge density and the strong electrostatic field [10]. On the other hand, when the relative humidity is high, lots of water layers will be formed which will leads to the formation of continuous water layer on the surface of sensor [15]. Furthermore, two conditions mentioned above (the nano-scale grain size and large specific surface area of the particles) also have a key role on the performance of sensor [16]. For the doped sensor, the average particle size and specific surface area are 15.98 nm and  $106.53 \text{ m}^2 \text{ g}^{-1}$ , respectively. Both values are much better than those of pure  $\text{ZrO}_2$ . In a word, the sensing properties of  $\text{ZrO}_2$  can be effectively controlled by doping  $\text{Sm}_2\text{O}_3$ .

## Conclusions

Humidity sensing properties  $\text{ZrO}_2$  doped can effectively control the performance of humidity sensing. By contrast, the  $\text{ZrO}_2$  doped with  $\text{Sm}_2\text{O}_3$  sensor shows better sensing characteristics (high sensitivity, fast response and recovery time) than pure  $\text{ZrO}_2$  sensor in the relative humidity range of 11 to 95% with 100 Hz. This fact can be explained by the higher specific surface area and larger adsorption capacity of water molecular resulted from  $\text{Sm}^{3+}$  substitute the site of  $\text{Zr}^{4+}$ .

## Acknowledgments

This work was supported by the National Natural Science Foundation of China under Grant no. 11404032.

## References

- [1] X.Q. Fu, C. Wang and H.C. Yu, Fast humidity sensors based on CeO<sub>2</sub> nanowires, *Nanotechnology*. 18 (2007) 145503-145506.
- [2] W. Strunk Jr and E.B. White, *The Elements of Style*, third ed., Macmillan, New York, 1979.
- [3] S. Yin and Z. Huang, Performance monitoring for vehicle suspension system via fuzzy positivistic C-means clustering based on accelerometer measurements, *IEEE/ASME Transactions on Mechatronics*. 20 (2015) 2613-2620.
- [4] M. Su, J. Wang and Y. Hao, Development of Y<sup>3+</sup> and Mg<sup>2+</sup>-doped zirconia thick film humidity sensors, *Materials Chemistry and Physics*. 126 (2011) 31-35.
- [5] S. Yin and X. Zhu, Intelligent particle filter and its application on fault detection of nonlinear system, *IEEE Transactions on Industrial Electronics*. 62 (2015) 3852-3861.
- [6] H.X. Li, Z.M. Shi and H.W. Liu, Humidity sensing properties of La<sup>3+</sup>/Ce<sup>3+</sup>-doped TiO<sub>2</sub>-20 wt.% SnO<sub>2</sub> thin films derived from sol-gel method, *Journal of Rare Earths*. 28 (2010) 123-127.
- [7] M. Anbia and S.E.M. Fard, Humidity sensing properties of Ce-doped nanoporous ZnO thin film prepared by sol-gel method, *Journal of Rare Earth*. 30 (2012) 38-42.
- [8] C.J. Wang, Y. Wang and Y. Cheng, Synthesis of monodispersed La<sub>2</sub>Ce<sub>2</sub>O<sub>7</sub> nanocrystals via hydrothermal method: a study of crystal growth and sintering behavior, *International Journal of Refractory Metals and Hard Materials*. 31 (2012) 242-246.
- [9] S. Yin, X. Zhu and O. Kaynak, Improved PLS focused on key performance indicator related fault diagnosis, *IEEE Transactions on Industrial Electronics*. 62 (2015) 1651-1658.
- [10] S. Yin and O. Kaynak, Big data for modern industry: challenges and trends, *Proceedings of the IEEE*. 102 (2015) 143-146.
- [11] C. Wang, Y. Wang, Y. Cheng, W. Huang, X. Fan, Y. Zhao, Y. Wang, B. Zou and X. Cao, Preparation and thermophysical properties of nano-sized Re<sub>2</sub>Zr<sub>2</sub>O<sub>7</sub> (Re=La, Nd, Sm and Gd) ceramic with pyrochlore structure, *Journal of Materials Science*. 47 (2012) 4392-4399.
- [12] R. Schaub, P. Thostrup and N. Lopez, Oxygen vacancies as active sites for water dissociation on rutile TiO<sub>2</sub> (110), *Physics Review Letters*. 87 (2001) 266104/1-266104/4.
- [13] S. Yin, X. Li, H. Gao and O. Kaynak, Data-based techniques focused on modern industry: an overview, *IEEE Transactions on Industrial Electronics*. 62 (2015) 657-667.
- [14] Y. Zhang, W. Fu, H. Yang, M. Li, Y. Li, W. Zhao, P. Sun, M. Yuan, D. Ma, B. Liu and G. Tian, A novel humidity sensor based on Na<sub>2</sub>Ti<sub>3</sub>O<sub>7</sub> nanowires with rapid response-recovery, *Sensors and Actuators B*. 135 (2008) 317-321.
- [15] H. Y. Jin, N. Wang, L. Xu and S. Hou, Synthesis and conductivity of cerium oxide nanoparticles, *Material Letters*. 64 (2010) 1254-1256.
- [16] J. Wang, M. Su, J. Qi and L. Chang, Sensitivity and complex impedance of nanometer zirconia thick film humidity sensors, *Sensors and Actuators B*. 139 (2009) 418-424.